Energy Storage and Conversion 2026, 4(1), 4098.
doi: https://doi.org/10.59400/esc4098

Article

Solar box cooker dehydration of culinary leaves: Leaf morphometrics and relative humidity endpoint detection

Victor John Law[1,*], James F. Lalor[2], Jenny Magnes[3], Denis Pius Dowling[1]

[1] School of Mechanical and Materials Engineering, University College Dublin, D04 V1W8 Dublin, Ireland
[2] School of Mechanical Engineering, Technological University Dublin, D01 K822 Dublin, Ireland
[3] Physics and Astronomy Department, Vassar College, New York, NY 12604, USA
*** Corresponding author:** Victor John Law, viclaw66@gmail.com

CITATION

Law VJ, Lalor JF, Magnes J, et al. Solar box cooker dehydration of culinary leaves: Leaf morphometrics and relative humidity endpoint detection. Energy Storage and Conversion. 2026; 4(1): 4098. https://doi.org/10.59400/esc4098

ARTICLE INFO

Received: 14 February 2026
Revised: 15 March 2026
Accepted: 20 March 2026
Available online: 25 March 2026

Abstract: Open solar dehydration has been used traditionally to remove moisture from culinary leaves in order to preserve their medicinal and nutritional qualities. This paper investigates the performance of a converted family-size (27 L) solar box cooker for solar dehydration of culinary leaves (Bay, Sweet, and Greek Basil and Common Sage). The investigation was carried out over the three month period from May to July 2025, on the island of Crete. The chosen leaves vary in their *in vivo* water content and leaf-blade morphology. The leaves are vertically triple-stacked within the dehydrator, and a green agricultural shadow-mesh cover is used to prevent direct solar irradiance damage. By performing solar dehydration during the day, leaf dehydration stress characteristics are identified. Solar dehydration parameters reported are: air temperature, relative humidity as a function of process time, leaf mass pre- and post-dehydration, and leaf water stress outcome in terms of visually observed leaf morphological changes (leaf rolling score and leaf shrinkage). For the top frame within the unloaded dehydrator, the relative humidity baseline follows a 4th-order polynomial time series 0D-model, with a extreme end behavior equilibrating to 8% relative humidity. Leaf-loaded studies reveal leaf water moisture is injected into the dehydrator, thereby linearizing the unloaded dehydration curve. Over a 3 to 7.5 h period of sunlight exposure, the top frame leave average a weight loss of 4.0 to 4.5 g per hour. For the partially sun blocked leaves on the middle and bottom frames, a supervised endpoint model is used, required adding approximately 1 h to account for the longer drying time.

Keywords: direct solar dehydrator; leaf dehydration; endpoint detection

1. Introduction

Open solar dehydration of freshly picked herbs has been a traditional way to preserve the medicinal and nutritional qualities of leaves when leaf supply becomes scarce and to reduce leaf weight for transportation (Kerr [1]). The solar preservation process utilizes both heat and mass transfer to remove the available water from the leaves, preventing microbial activity that would spoil the leaves' medicinal, nutritional, and flavor value. Today, direct-solar dehydrators (DSD) and indirect-solar dehydrators (ISD) employing passive air-flow, with inlet air-filters to reduce windblown dust, pests, and germ contamination, are used to increase the production of solar dehydration of culinary leaves (Hassanain [2], Imam et al. [3], Ouafi et al. [4], Shalaby et al. [5], Jayasuriya et al. [6], Bennamoun et al. [7], Ndukwu et al. [8] and Tonadi et al. [9]).

The agricultural scale DSD are generally considered to be a sustainable and eco-friendly alternative to ISD (Papu et al. [10], Akbar et al. [11], and Dhande et al. [12]), but may be financially out of reach for the small family unit, however the solar box cooker, with or without external panels to reflect sunlight into the box and converted to a drier is more affordable [1]. N.B. electric ovens and microwave dryers [13] are not considered here as they are generally less sustainable, or, less eco-friendly than off grid solar dryers. A good example of a SBC converted to dry fruit has been reported by, Abdulmujeeb et al. [14] where 4 to 5 mm thick banana slices were dehydrated at temperatures of 40–88 ℃ for 8–9 h. More recently, a converted SBC (Law et al. [15] and Lalor et al. [16]) for solar dehydration of Bay leaves (Laurus nobilis) from a female Bay shrub (Law et al. [17]) has been reported. However, there is concern that DSD can create a spatial dehydration discrepancy within the solar dehydrator and impacts negatively on leaf color and biochemical composition, due to the action of transmitted sunlight through the transparent window onto the leaves (Hassanain [2], Danso-Boateng [13], and Kumar et al. [18]). To reduce this problem researchers have reported on the use of colored (blue or yellow) glass windows to restrict the solar wavelength energy reacting with the target leaf product [8], or reducing solar irradiance intensity transmitted through the glass window by employing a covering of agriculture shadow-mesh. In the latter two cases; black colored shading cloth is used to reduce solar irradiance by some 50% when dehydrating Common Sage leaves (Salvia officinalis L.) in Ismailia, Egypt [2]; and green agricultural shadow mesh for reducing solar irradiance by approximately 60 % when dehydrating oregano leaves in Tabasco, Mexico (Castillo-Téllez et al. [19]). Using the green agricultural shadow-mesh approach, Bay leaves can be dehydrated at air temperatures of 40–55 °C within 2–3 h without visual signs of leaf rolling [17]. These DSDs use the open-greenhouse principle to remove accumulated heat and moisture by natural airflow via inlet and outlet ventilation holes. Thus, when leaves are placed within the DSD, the impact of solar energy warms and releases the available leaf water moisture, then carries the moisture away from the leaf surface, where warm buoyant flowing air carries the moisture out at the top of the DSD. In this leaf configuration, the DSD is said to be ‘loaded’, and when the DSD is empty (no dehydration frames or leaves), it is said to unloaded. Therefore by, monitoring and comparing the time evolving relative humidity (RH) and temperature profile of the loaded and unloaded DSD a non-invasive real-time insight into the leaf dehydration process may be made. The novelty of this approach is that monitoring can be made in real-time with minimal equipment, as opposed to the invasive approach of repeatedly taking leaves out of the solar dehydrator to measure their water loss. A further benefit of this monitoring approach is that valuable sunshine energy is not released from the DSD during repeated leaf weighing, therefore potentially reducing the solar dehydration from days to a single day where no overnight leaf rehydration is encountered.

In this work the DSD is converted solar box cooker, and henceforth called SBC-d, where ‘d’ denotes the dehydration conversion, is an off-grid device that is an example of sustainable Green technology, as it does not use portable electricity units, gas, or oil bought in cylinders, nor photovoltaic cells, as a source of enabling energy. Even

with these eco-friendly accolades, the challenge of reducing direct solar irradiance on leaves placed on the top frame while leaves on the intermediate and bottom frames are partially blocked from the Sun's impinging energy generates uneven drying times.

The aim of this work is fourfold.

1) Use non-invasive real-time RH and temperature measurements to characterize a family sized (27 L) SBC-d. Acknowledging that changes in RH as a "leaf moisture component is likely to be sensitive to ambient variability, leakage/ventilation, and temperature effects, a single SBC-d with green agricultural shadow-mesh covering for the purpose of leaf dehydration is used on the island Crete (35.31° N, 24.31° E, altitude 150 m) during the months May through July 2025.
2) To visually identify leaf solar dehydration morphological induced changes (leaf rolling and shrinkage) of four different culinary Lamiaceae leaf types within the SDC-d.
3) Develop a leaf dehydration endpoint methodology on RH and temperature data complied within Microsoft Excel software that compares historical real-time unloaded (empty) with real-time loaded (leaf), followed by an A minus B mathematical operation of the two datasets to reveal the difference that may be related to the leaf water moisture injected into the SDC-d. The mathematical operation is based on the processing of complex datasets as described by Law and Dowling [20,21].
4) Develop a state-space-model (SSM) [22] using the experientially determined leaf rolling score and leaf shrinkage score as state variables as a function of solar dehydration time to quantify leaf hydroresponse to the SBC-d operating environment. Using this approach to quantify the difference between the four leaf genera studies, using these results to classify leaf response to SBC-d induced stress environment.

2. Description of the Lamiaceae leaves

The leaves used in this study are from the Lamiaceae, an member of mint family, which is one of the largest and diverse groups of flowering plants comprising over 7,000 species across 250 genera (Uikey [23] and Joshi et al. [24]. The leaves are important to humans as they have wide ethno-medicinal use due to their temperature sensitive bioactive compounds (essential oils, flavonoids, terpenoids, and polyphenols) which give them their aromatic taste, fragrance, and medicinal properties. The four leaves are: Sweet Basil (*Ocimum basilicum*—from the Greek words meaning 'smell' and 'kingly herb') **Figure 1a**, its cultivar Greek Basil (*Ocimum basilicum* var, minimum—from Latin and Greek words meaning: 'small', 'smell', and 'kingly herb') **Figure 1b**, Common Sage (*Salvia officinalis*—from the Latin words: 'to heal' and 'herb store', or 'pharmacy') **Figure 1c**, and Bay (*Laurus nobilis*—translated from Latin to 'praiseworthy noble'). **Figure 1d**, and with care, can be grown as annual, or at the very least, perennial. In each case, the leaves emerge from square stems and are ovate in shape with a midrib and pinnate vascular bundles. The primary reason for this selection is their range in water moisture content (28 to 78%) and variation in leaf-blade rigidity (Bay being the most ridged, Basil being least ridged).

Figure 1. Lamiaceae shrubs. **(a)** *Ocimum basilicum*; **(b)** *Ocimum* basilicum var, minimum; **(c)** *Salvia* officinalis; **(d)** *Laurus nobilis*.

The Bay leaves were hand-picked from a mature female Bay that is exposed to the full Eastern Mediterranean Sun. The leaves have an ovate shape and have fully differentiated adaxial (top) and abaxial (underside) surfaces with a bi-curvature midrib measuring typically 2 × 2 mm at the leaf base. The leaf's secondly branching pinnate vascular bundles also protrude through the abaxial. Held in the hand, they have a semi-ridged feel, but break when bent too far. At the Microscopic level (Serebrynaya et al. [25]), living collenchyma and lignified sclerenchyma cells, which are dead at maturity, provide stiffness and support to the vascular bundles and protection to the water-filled bulliform cells, water storage, and gas storage in spongy mesophyll cells under abiotic stress conditions. Additionally, a cuticle layer on the adaxial epidermis produces the characteristic olive-green glabrous leaf color. The abaxial epidermis has spatially separated stomata cells, giving it its characteristic dull green color.

Sweet Basil leaves are hand-picked from a bush that is grown in partial shade. The leaves are typically 5 cm in length and 1.6 cm in width, with the midrib typically measuring 1.8 × 18 mm at the leaf base, and secondary branching pinnate vascular bundles that visibly protrude into both sides of the leaf-blade. The leaves are bright green in color, with a prominent downward curvature and tender; breaking easily when rolled in hand, yielding a mixture of fragrant oil and water. When fresh, the leaves have an approximate water content of 86% [5]. Microscopy studies (Pysklynets and Makhinya [26]) reveal that they have diacytic stomata and eight-celled essential oil glands and collenchyma cells that provide the leaf flexibility. As a comparison, the leaves of the Greek Basil cultivar with their smaller leaf area are used.

The Sage leaves are hand-picked from a Common Sage bush growing in partial shade. The leaves are flexible when rolled in the hand, but do not crush easily when compared for example to Basil leaves. Their adaxial is grey-green in color with spatially spaced short trichomes (hairs) that regulate water retention, whereas the abaxial is

revealed to have full venation (midrib, secondary branching pinnate vascular bundles, and tertiary reticulated venule vascular bundles). Typically, the leaves have a water content of approximately 76 ± 1% [2,3]. In addition, microscopy studies (El-Sahhar et al. [27] and Özdemir et al. [28]) reveal extensive collenchyma cells around the midrib and pinnate vascular bundles.

Table 1 lists the average leaf morphology (midrib cross-section, leaf length and width, leaf area, and fresh leaf water content).

Table 1. Average leaf morphology characteristic prior to solar dehydration.

Leaf	Midrib cross-section at leaf base (mm)	Average leaf L × w (cm)	Average leaf area (cm^2)	Average leaf water content (%)
Laurus nobilis	2 × 2	6 × 2.5	47.12	~28
Ocimum basilicum	1.5 × 1.5	4 × 1.6	20.1	~86
Oci*mum basilicum* var, minimum	1.2 × 1.2	2 × 0.8	5	~86
Salvia officinalis	1.8 × 1.8	5 × 2	31.4	~75–78

The woody perennial aromatic evergreen shrubs, thyme and rosemary, are not considered here, as their woody stems are required to hold their ovate or needle-like leaves together within the SBC-d dehydration frames, thereby complicating weight and water moisture calculations.

3. Experimental

3.1. SBC-d build cost and weight

The construction cost of the family sized (27 L) SBC-d was 162 Euro (May 2025). The cost includes materials and labor at the local carpentry workshop and the farm metal workshop. When adjusted for US dollars (exchange rate 1.1), the cost equates to 178.2 US dollars. In terms of weight (including the metal tripod), the SBC-d weight is some 18.2 kg.

3.2. Leaf mass and target leaf water content loss

All the leaves in this study were hand-picked a few hours before each solar dehydration experiment from plants grown in the family garden. Dust and pests are removed from the leaf surfaces by rinsing in water, and then cloth dried leaving an additional weight of water that has been absorbed through the leaf stomatas, the petiole open end, and residual water on leaf surfaces. The leaf target water (moisture) loss is obtained by first calculating the difference between the initial batch leaf mass (m_0) and the increased weight (m_1) of the batch after the cleaning process. Equation (1) determines the leaf batch water mass gain ($m_{water\ gained}$).

$$m_{water\ gained} = m_1 - m_0 \tag{1}$$

Using this knowledge and the average *in vivo* leaf water content for each leaf type [2,3,5,17,18], the target water loss is then calculated (**Table 2**).

Table 2. Leaf batch mass data.

Leaf genera	Average leaf water content (%)	m_0 (g)	m_1 (g)	$m_{water\ gained}$ (g)	Target water loss (g)
Laurus nobilis	~28	27	30	3	12–13
Ocimum basilicum	~86	24	31	7	26–27
Ocimum basilicum var, minimum	~86	34	38	4	29–30
Salvia officinalis	~75-78	30	40	10	34–35

3.3. Leaf dehydration frame loading

Three dehydration frames with open lattice mesh (584 cm^2) are used in this study. The frames are triple-stacked within the SBC-d (**Figure 2a**). On each frame, leaves are arranged adaxial side-up in three rows, typically leaving a surrounding area equal to the ventilation outlet area air (240 cm^2) for the warm buoyant air to pass through **Figure 2b**.

(a) **(b)**

Figure 2. **(a)** 3D cross-section drawing of SBC-d; **(b)** Photograph of dehydration frame with three rows of 6 Bay leaves: total 18 leaves.

3.4. Relative humidity, temperature, and wind speed measurements

In this study, a stainless-steel analogue-dial temperature probe with a range of 0 to 100 ℃ and an accuracy of 1 ℃, is used to measure the SBC-d air temperature (T_{air}) at the top dehydration frame. A further digital thermometer with an accuracy of 0.1 ℃ is used to measure the outside ambient temperature within the shade. A ThermoPro HR monitor with an accuracy of 2–3% is placed on the top dehydration frame to measure the SDC-d HR. In this case the HR measurement is the ratio of actual atmospheric moisture to the maximum amount of atmospheric moisture at a given T_{air}, expressed as a percentage (%). Local wind speed was obtained by consulting weather.com App, and was found to be generally light (0–10 $km.h^{-1}$). Using this approach a 0D-model (having no spatial dependency other than probe measurement as a function of time) of the leaf dehydration process can be generated.

3.5. Temperature and relative humidity (RH) time series curve fitting

Microsoft Excel spreadsheet is used to collate the time series experimental data and dimensionally reduce the data for visualization as an XY scatter plot [20,21]. Facets, shape, and color are used to delineate the leaf type, RH, and temperature measurements. Each time series data presents an increasing (or decreasing) non-linear curve with

end behavior extending to infinity. Regression trend-line functions (logarithmic and power functions that have one deflection or polynomial function, up to the 4^{th} order, is used to generate a zero-dimensional model (0D-model). Here it is noted that 4^{th} order and higher orders may provide a statistically strong fit, they often lack physical interpretability. This study therefore explores whether the chosen regression function corresponds to actual physical processes. During the Excel regression a linearization algorithm is used to model the data by logarithm transformation, followed computation approximation of the coefficient of determination (R^2) (Yurdakul et al. [29] and Buzrul [30]). With this approach, the SBC-d RH and temperature data best-fit trend-lines are constructed for a.m. time-stamped data (where the Sun's altitude is increasing along with solar irradiance with one embedded deflection), and for p.m. time-stamped data (where the Sun's altitude decreases along with solar irradiance from solar noon, producing a second embedded deflection). Of particular interest here is the non-linear RH and temperature data which includes a local deflection time-stamped at t = 9 a.m. when opening and closing of the SBC-d window; in this scenario, a polynomial function approach is more flexible (Hernández et al. [31]) than a logarithmic or power function. It is also noted that the best-fit 0D-model as measured by R^2 highlights short period/local variance, but this unsupervised approach sometimes requires a supervised approach to match real-world underlying process mechanisms. To allow researchers easy access to all of the regression analyses function performed are complied in **Appendix A** for future reference.

The A minus B mathematical operation is performed by entering values of the loaded RH time series data into column A and entering the unloaded RH baseline data into column B; Excel then performs the A minus B array calculation to generate the third column (D) that represents the leaf moisture component injected into the SBC-d as a function of time.

3.6. SBC-d azimuth positioning

Prior to leaf solar dehydration, the SBC-d is manually aligned to Sun azimuth position every 15 to 20 min to preheat the box's internal volume to a measured 40–45 ℃, and measured RH to 45–55%. With this criterion met, the room-temperature (22 to 24 °C) triple-stacked frames, with or without leaves, are inserted into the SBC-d. As the aim is to dehydrate, not cook, the SBC-d is then aligned to the Sun's azimuth position every half-hour. Monitoring of the solar dehydration process is carried out as a function of time for the following parameters: number of dehydration frames (3), SBC-d internal air and absorber temperature, RH, and solar irradiance. When the solar dehydration process is deemed to be finished, the frames are taken out and the leaves are weighed to calculate leaf water loss and their change (if any) in leaf morphology is recorded.

3.7. Leaf water content

To extract the leaf water content from the solar dehydration measurement, an A–B transformation is performed in the spreadsheet by subtracting the RH-loaded time series data from the previous day, or the averaged unloaded time series data. For example, the

values in column B, rows 2 to 36, are subtracted from the values in column C, rows 2 to 36, with the result placed in column D, rows 2 to 36.

3.8. Leaf rolling score

Half of the world's population consumes rice (*Oryza sativa* L.) that it grown in flooded paddy fields. For many years it has been known that when rainfall is insufficient in the growing season rice leaves begin to exhibit morphologic changes due to water, or drought, stress in the form of wheat/rice/leaf rolling score (Ali et al. [32], Yavas et al. [33], Fen et al. [34], Latif et al. [35] and Guo et al. [36]). This is evaluated based on a score which ranges from 0 = normal growth to 5 = maximum stress. This established scalar water stress index is used as a basis for characterizing leaf morphology change due to the solar dehydration environment within the SBC-d. To enhance leaf morphology change characterization, the onset of leaf shrinkage is the time-stamped and its duration is measured to the start of leaf rolling. [To the knowledge of the authors, this latter characterization is absent in the rice leaf rolling score]. With this dual characterization within a fixed solar dehydration environment (SBC-d with an agriculture shadow mesh covering at a location), Lamiaceae leaf genera allometry is performed to generate a state-space, where LLRS is plotted on the vertical axis and solar dehydration time is plotted on the horizontal axis. Here, the morphometrics (Klingenberg [37]) enable both leaf rolling and the shrinkage vector that is characteristic of the leaf genera and the vector relationship between leaf genera. The advantage of such a vector graphic is its ability to visualize the leaf's physical response to the solar dehydration process.

4. Lamiaceae solar dehydration study

4.1. Bay leaf solar dehydration

Figure 3 presents the SBC-d and agricultural shadow-mesh study of unloaded triple-stacked frames and triple-stacked frames loaded with 30 g (fifty-four leaves) of Bay leaves. The solar preheating started at t = 8 a.m. and finished at t = 9 a.m. For reference, the unloaded T_{air} and ambient temperature time series curves are shown.

The first notable is that the unloaded T_{air} increases non-linearly with time from 24 to 57 ℃ without a secondary deflection when the window is open and closed. Excel trend-line coefficient of determination varied from R^2 = 0.9922 for a natural logarithm function, R^2 = 0.9808 for the power function, and R^2 = 0.9683 for the 2nd-order polynomial function; the logarithm and power coefficients are tabulated **Appendix A**. Using this regression analysis, the air temperature profile is most likely to follow either a natural logarithm function or a power function with a single deflection.

The second feature of note is that the unloaded RH curve shows similar behavior during the preheating stage (45% at 8 a.m. to 25% at 9 a.m.). After which RH values fall more rapidly than the loaded curve until reaching an equilibrium level with a long tail finishing at 2 p.m. The trend-line function fitting procedure yields a regression analysis ranking; R^2 = 0.9835 for the 4th-order polynomial function, R^2 = 0.9291 for the power function, and R^2 = 0.8903 for a natural logarithm function. Using this

analysis, the unloaded data indicates that the dehydration process most likely follows a 4th-order polynomial function, where the initial time period (8 to 9 a.m.) represents the SBC-d internal moist air is removed followed by moisture from the SBC-d walls. see **Appendix A** for logarithm and power coefficients.

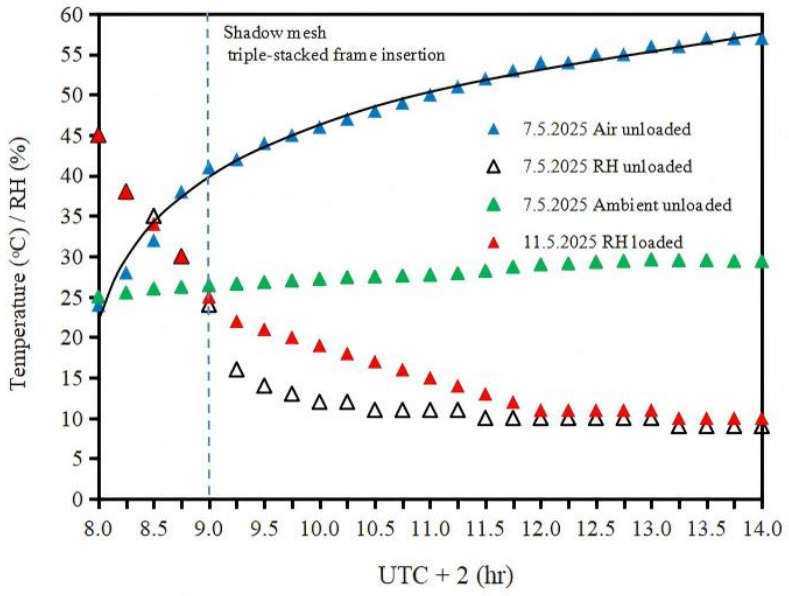

Figure 3. SBC-d and agricultural shadow-mesh dehydration of Bay leaves, fifty-four leaves in the triple-stacked frames.

Note: Unloaded RH = open triangles, unloaded T_{air} = blue triangles with a natural logarithm trend-line (R^2 = 0.9922), and Unloaded T_{amb} = green triangles, 7.5.2025. Loaded RH = red triangles, 11.5.025 with solar irradiance varying from 853 to 1004 W·cm^{-2}.

The third feature of note is that the loaded RH curve appears to have three characteristic dehydration periods (8 to 9 a.m., 9 a.m. to 12 p.m., and 12 to 2 p.m.) that start with RH = 45 % at 8 a.m. and finish at RH = 10 % at 2 p.m. At the end of the dehydration time (2 p.m.), the leaf mass loss is 40 %, which equates to water loss of 12 g. For this curve, the trend-line function fitting procedure yields a best-fit ranking: R^2 = 0.9949 for the 4th-order polynomial function, R^2 = 0.9859 for a natural logarithm function, and R^2 = 0.9695 for the power function (see **Appendix A** for logarithm and power coefficients). Using this regression analysis, there is no clear dehydration logarithmic or power function for dehydration; rather, the process follows a smoothed quasi-linear function.

It is important to note that no power law can be established, as the data range on the x-axis is only 1 order of magnitude (Stumpf and Porter [38] and Andriani and McKelvey [39]). This regression analysis is further explored in the Basil and Common Sage leaf dehydration experiments.

Figure 4 reveals the result of the A minus B Excel computation as a function of time. Here, the initial preheating time period (t = 8 to 9 a.m.), reveals that the change in RH is relatively stable (0 ± 1%), after which the change in RH rapidly increases to 7 ± 1% between t = 9.5 and 10 a.m. From this point forward, the change in RH falls at a rate of 3% per hour, with RH values equilibrating to the unloaded SBC-d RH level from 12 a.m. to 2 p.m. At 12 h the leaves in the top frame are still semi-ridged and flexible with a rolling score = 0 to 1, and a rolling score = 2 at 12.30 a.m. At 1 p.m.,

the rolling score = 3 with the leaves having a crisp texture that breaks when handled between thumb and forefinger. At this score, the leaves are unsuitable for direct culinary use as broken leaves are a choke hazard in the mouth and the potential to cut soft tissue. A Photographic comparison of fresh Bay and solar dehydrated Bay leaves is given in **Figure 5**.

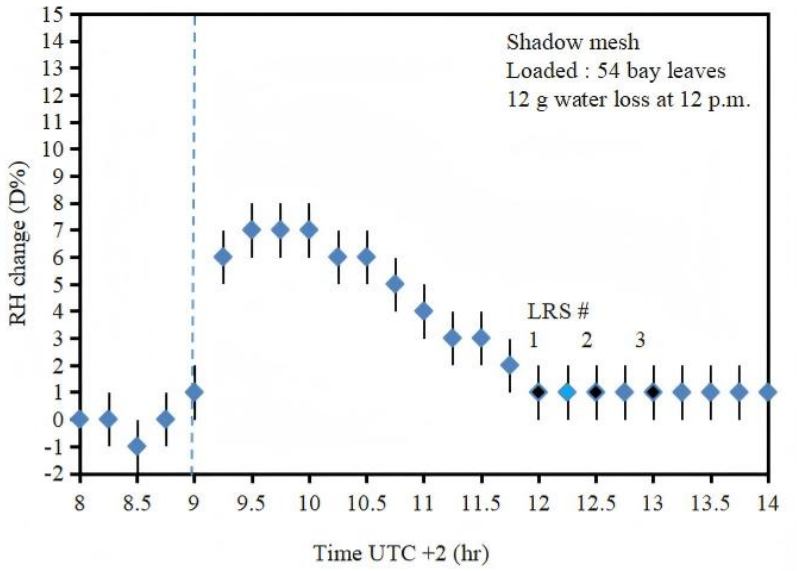

Figure 4. SBC-d and agricultural shadow-mesh solar dehydration A minus B RH times series data for fifty-four Bay leaves in triple-stacked frames. Note: Black-filled diamonds denote LLRS observations.

A Photographic comparison of fresh Bay and solar dehydrated Bay leaves is given in **Figure 5**.

(a) **(b)**

Figure 5. **(a)** Photographs of solar-dehydrated Bay leaves. Fresh leaves; **(b)** solar dehydrated leaves.

4.2. Sweet Basil leaf solar dehydration

Figure 6 presents the SBC-d and agricultural shadow-mesh study of unloaded triple-stacked frames and frames loaded with 31 g of washed Sweet Basil leaves. The same solar preheating timing (t = 8 to 9 a.m.) is used as in the Bay leaf study. However, due to the 86% leaf water content, the Sweet Basil leaves require approximately 7 h (9 to 2.30 p.m.) of dehydration time which equates to a treatment time of approximately 1.5 h passed solar noon. For reference, the unloaded T_{air} and ambient temperature time series curves are shown.

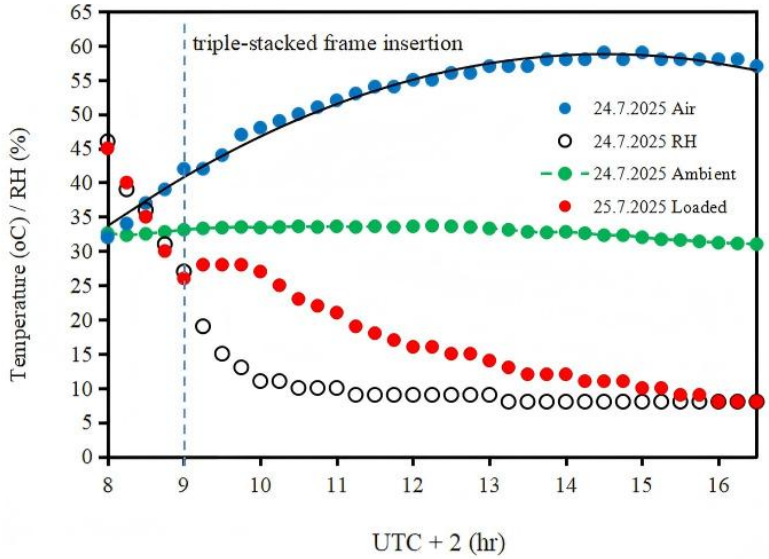

Figure 6. SBC-d and agricultural shadow-mesh dehydration of Sweet Basil leaves loaded in triple-stacked frames.

Note: Unloaded RH = open circles, unloaded T_{air} = blue circles with 2nd-order polynomial trend-line (R^2 = 0.9892), and Unloaded T_{amb} = green circles, 24.7.2025. Loaded RH = red circles 25.7.2025; solar irradiance varying from 853, through solar noon 1,020, to 879 W·cm^{-2} at 2.30 p.m.

Under these conditions, the unloaded T_{air} curve exhibits a nonlinear time behavior from 32 ℃ at 8 p.m., 59 ℃ at solar noon, then falling to 55 ℃ at the end of the study period. For this dataset, the trend-line coefficient of determination varied from R^2 = 0.9892 for the 2nd-order polynomial function, R^2 = 0.9694 for the power function, and R^2 = 0.9686 for a natural logarithm function. The logarithm and power coefficients are tabulated in **Appendix A.**

The unloaded RH data reveals a non-linear falling curve behavior, i.e., a rapidly falling initial period followed by reaching an equilibrium level of RH = 10% at 11 a.m. and finishing with a long tail at 4.30 p.m. Here it is reasonable to assume the initial slope (8 to 9 a.m.) represents the moisture diffusion rate of the empty SBC-d, after which the slope depends on the additional moisture content of the leaves from all three frames. The best-fit trend-line coefficient is: R^2 = 0.9872 for the 4th-order polynomial function, R^2 = 0.9076 for the power function, and R^2 = 0.8516 for the natural logarithm function. See **Appendix A** for logarithm and power coefficients.

The loaded RH time series data, the preheating curve are similar to those in **Figure 3**, but after the loaded frames are inserted, RH increases and spikes with RH = 28% between 9.15 and 9.75 a.m., from where RH values decrease gradually to RH = 10% at 2.0 p.m. and finally reach equilibrium at 4.30 p.m. At this point, the leaf mass

is reduced by 86%, or 27 g, at a rate of loss of 3.8 g per hour. In terms of best-fit trend-line coefficient, $R^2 = 0.9757$ for a 4th-order polynomial, or $R^2 = 0.975$ for the natural logarithm function. The difference reported is a significant figure that brings into focus the true accuracy of the linearizing transformation algorithm [29,30]. Finally, the power function produces the worst fit with $R^2 = 0.89$. See **Appendix A** for logarithm and power coefficients**.**

Figure 7 reveals the result of the A minus B Excel computation as a function of time. Again, the preheating stage t = 8 to 9 a.m. is similar to those shown in **Figure 4**, where the change RH value is relatively stable (0 ± 1%). From this time-stamp the change in RH rapidly increases to 16% at t = 10 a.m. From this point forward the change in RH falls at a rate of some 2.5% points per hour, where at t = 4.p.m., the RH values equilibrate to the unloaded SBC-d RH level. The annotation depicts the observed onset of leaf collapse and accompanying shrinkage, followed by leaf rolling response to the solar dehydration process. In this case, at approximately four hours into solar processing, leaves are observed to shrink in area, followed by signs of rolling, with a rolling score = 1 at 2.p.m., rolling score = 2 at 2.25 p.m. By t = 4 p.m., the top frame leaves are judged to have reached their target water mass loss of 27 g or 86% of their total mass. **Figure 8** shows a comparison of freshly picked Sweet Basil and 5 h of solar dehydration *(t* = 2 p.m., **Figure 7**).

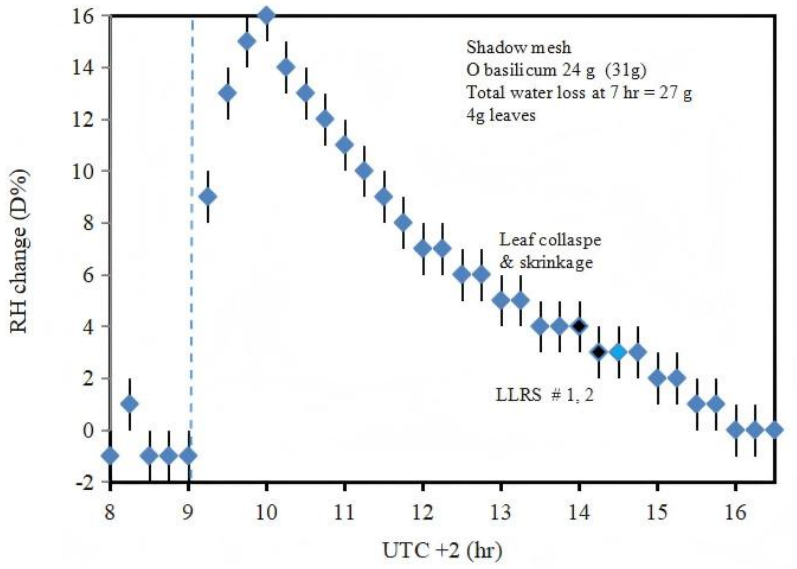

Figure 7. SBC-d and agricultural shadow-mesh solar dehydration of Sweet Basil in triple-stacked frames: A minus B RH times series data.

Note: Black-filled diamonds are LLRS observations.

4.3. Greek Basil leaf solar dehydration

Figure 9 presents the SBC-d and agricultural shadow-mesh study of unloaded triple-stacked frames and frames loaded with 38 g of washed Greek Basil leaves and stems. Again, the solar preheating stage is the same as the Bay and Sweet Basil study (8 to 9 a.m.). With 86% leaf water content (the same as Sweet Basil), the dehydration process is some 7 h (9 a.m. to 4 p.m.), which equates to a treatment finishing time of approximately 1.5 h passed solar noon, where the Sun's altitude decreases along with

solar irradiance. For reference, the unloaded T_{air} and ambient temperature time series curves are provided again. In the case of T_{air}, it reaches a maximum of 59 ℃ at solar noon, and then falls to 57 ℃ at 4 p.m. Given that there are two deflections within the curve, a 2nd-order polynomial trend-line produces an R^2 = 0.9893. This can be compared to R^2 = 0.9756 for a natural logarithm, and R^2 = 0.9789 for a power function, see **Appendix A** for their logarithm and power coefficients.

Adaxial Abaxial LRS = 1, 2

Figure 8. Photographs of freshly picked Sweet Basil showing visible midrib and pinnate vascular bundles (left) and at 5 h of solar dehydration, *t* = 2 p.m (right).

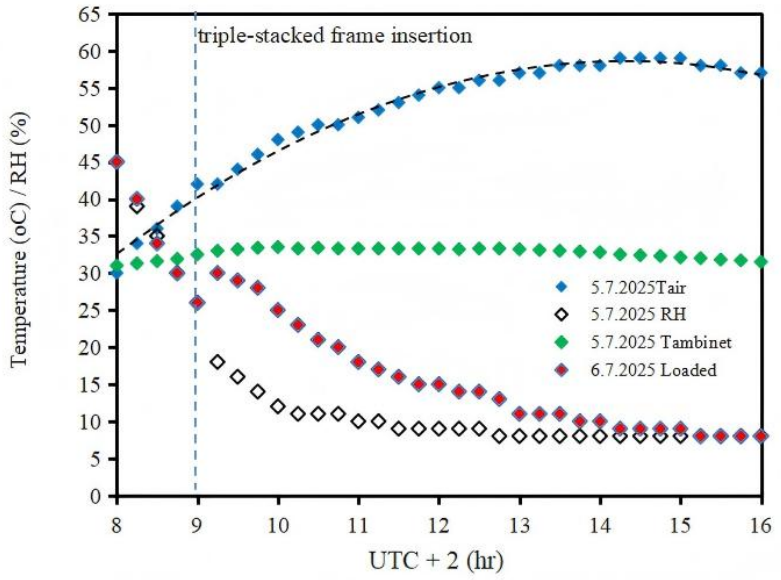

Figure 9. SBC-d and agricultural shadow-mesh dehydration of Greek Basil leaves in triple-stacked frames.

Note: Unloaded RH = open diamonds, unloaded T_{air} = blue diamonds with 2nd-order polynomial trend line (R^2 = 0.9893), and Unloaded T_{amb} = green diamonds, 5.7.2025. Loaded RH = red diamonds 6.7.2025; solar irradiance varying from 853 W·cm^{-2}, through solar noon (1,025 W·cm^{-2}) to 1,020 W·cm^{-2} at 4 p.m.

The unloaded RH curve behavior is similar to the unloaded curves presented in **Figures 3** and **6**; that is a rapidly falling RH value, followed by a long tail with an equilibrium level of RH = 8% at 4 p.m. The trend-line here is the 4th -order polynomial function; R^2 = 0.9908, followed by the power function (R^2 = 0.9345 and then the

natural logarithm function (R^2 = 0.8903). See **Appendix A** for logarithm and power coefficients.

Moving on to the loaded RH time series data, the preheating curve is similar to **Figure 3**. But after the Greek Basil leaf frames are inserted, RH levels increase and spike to RH = 30–29% at 9.30 a.m., from where RH values decrease gradually to RH = 8% at 4 p.m. At this point, the leaf mass loss is 86% which equates to a water loss of 30 g at a rate of 4.6 g per hour. In terms of best-fit trend-line, R^2 = 0.9782 for a 4th-order polynomial, closely followed by R^2 = 0.974 for the natural logarithm function. The power function produces the least fit with R^2 = 0.9005. The logarithm and power coefficients for these curves are tabulated in **Appendix A**. Again, there is no clear logarithm or power function outcome, again pointing to a smoothed quasi-linear function.

Figure 10 reveals the result of the A minus B Excel computation as a function of time. Again, the preheating time period (t = 8 to 9 a.m.) is similar to **Figure 4**, where the ΔRH value is relatively stable (0 ± 1%). At this point, the leaves with stems on the stacked frames **Figure 11a** are inserted into the SBC-d. From this point onwards, ΔRH rapidly increases to 14 ± 1% between t = 9.5 and 10 a.m. From where the ΔRH decreases by 3 percentage points per hour for the next 2 h, then slows to a rate of 2 percentage points until the level matches the unloaded SBC-d RH level between 12 a.m. to 4 p.m. Note also that as the dehydration rate decreases to 2 percentages points per hour, the leaves lose turgor pressure and collapse from their 3-dimensional structure, forming a limp 2-diamensional structure **Figure 11b**. In this instance, the leaves begin to shrink in area after 4 h (t = 1 p.m.) of solar processing. By t = 2 p.m., the leaves exhibit a rolling score = 1, and by 12.25 a.m., a rolling score = 2 (annotated here as black-filled diamonds). At t = 4 p.m., the leaves are judged to have reached their target water mass loss of 30 g or 86% of their total mass; the remaining 8 g of chopped leaves **Figure 11c**, and the 1 g of stem material **Figure 11d.**

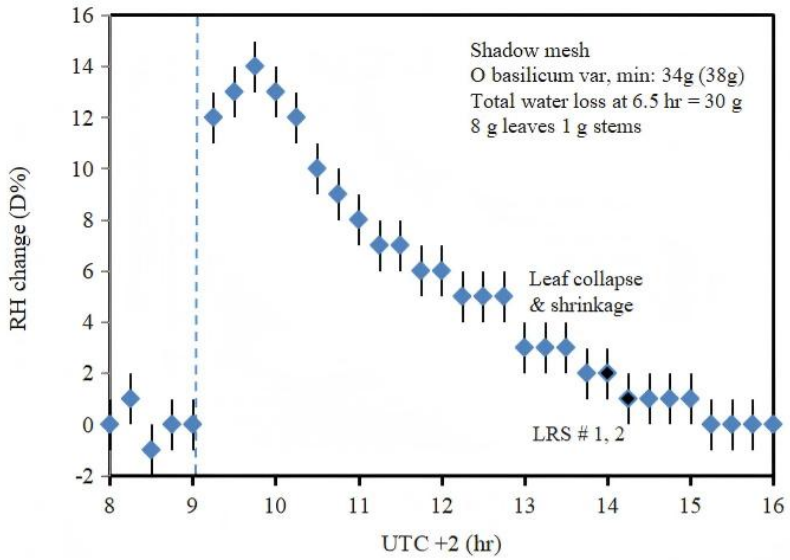

Figure 10. SBC-d and agricultural shadow-mesh solar dehydration A minus B RH times series data for Greek Basil leaves in triple-stacked frames.

Note: Black-filled diamonds are LRS observations.

Figure 11. Photographs of the four stages of solar dehydration of fresh Greek Basil leaves. **(a)** Fresh Greek Basil placed on dehydration frame; **(b)** collapse, and shrinkage of leaves; **(c)** chopped solar dehydrated leaves; **(d)** cut dehydrated stems.

4.4. Common sage leaf solar dehydration

Figure 12 presents the SBC-d and agricultural shadow-mesh study of unloaded triple-stacked frames and triple-stacked frames washed and loaded with 40 g of Common sage leaves. The solar preheating was performed between t = 8 and 9 a.m. The time series curves for the ambient temperature are also provided. With 76% leaf water content, the solar dehydration process took approximately 7.5 h (9 a.m. to 4.5 p.m.), which equates to a finishing time of approximately 2 h passed solar noon. In this study, T_{air} reaches a maximum of 59 ℃ at solar noon, then decreases to 58 ℃ at 4.5 p.m., generating a two-deflection time series curve, with a best-fit 2nd-order polynomial function (R^2 = 0.9911). A comparison with R^2 = 0.8814 for a natural logarithm, and R^2 = 0.8345 for a power function yields a poor fit. See **Appendix A** for their logarithm and power coefficients.

The unloaded RH time series curve again resembles the unloaded curves in **Figures 3**, **5**, and **8**. In this case, falling rapidly until reaching a near equilibrium level of 10% at 10.5 a.m., followed by a long tail finishing at the extreme end of 4.30 p.m., where

the RH = 8.5%. The best-fit trend-line yields $R^2 = 0.9841$ for a 4th-order polynomial. This was followed by $R^2 = 0.7471$ for the power function and $R^2 = 0.6211$ for the natural logarithm function. See **Appendix A** for logarithm and power coefficients.

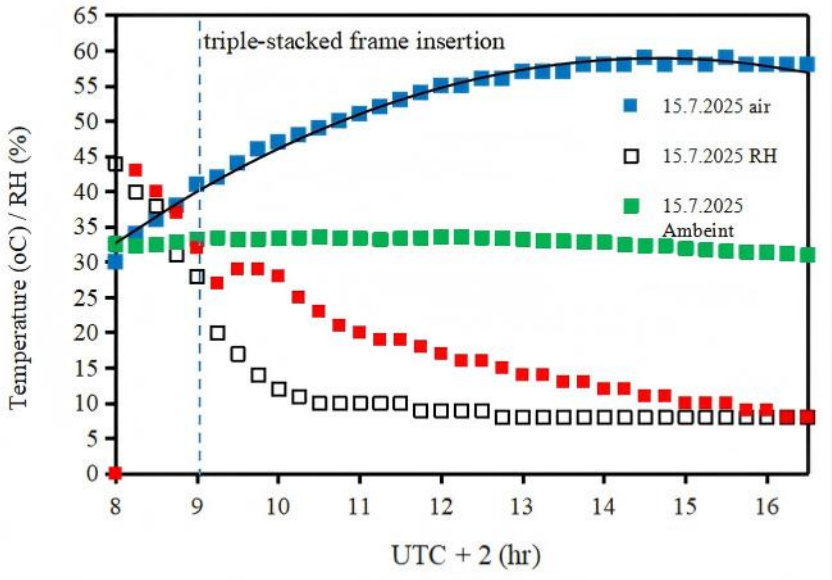

Figure 12. SBC-d and agricultural shadow-mesh dehydration of Common Sage leaves loaded in triple-stacked frames.

Note: Unloaded RH = open squares, unloaded T_{air} = blue squares with a 2nd-order polynomial trend-line ($R^2 = 0.9911$), and Unloaded T_{amb} = squares 15.7.2025. Loaded RH = red squares 16.7.2025; solar irradiance varying from 850 W·cm^{-2}, through solar noon (1,020 W·cm^{-2}), to 860 W·cm^{-2} at 4 p.m.

When the Sage leaves are inserted, there is an increase in RH, spiking at RH = 29% at 9.30 a.m., after which the RH value decreases gradually to RH = 8% at 4.5 p.m. At this point, the leaf mass loss is 76% which equates to a water loss of 34 g at a rate loss of 4.5 g per hour. Applying the best-fit trend-line, $R^2 = 0.9927$ for the power function, closely followed by $R^2 = 0.9888$ for the 4th-order polynomial. The natural logarithm function yields a $R^2 = 0.931$. The logarithm and power coefficients for these curves are tabulated in **Appendix A**.

Figure 13 presents the result of the A minus B Excel computation as a function of time. Here again, the preheating time period (t = 8 to 9 a.m.) is similar to **Figure 4,** where the change in RH is relatively stable (± 1%). Beyond this point, RH rapidly increases to 14 ± 1% between t = 9.5 and 10 a.m. From where the change in RH falls at a rate of −2.33 % for the next 6 h, then levels out to match the unloaded SBC-d RH value at 16.5 h. The Sage LRS is annotated along this curve. In this instance the the LRS = 3 at t = 3 p.m., rolling score = 1 at t = 12.5 a.m., rolling score = 2 at t = 2 p.m., and rolling score = 4 at t = 4 p.m. At t = 4.5 p.m., the leaves are judged to have reached their target water mass loss of 34 g or 76% of their total mass, a water mass loss rate of 4.5 g per hour. **Figure 14 s**hows the adaxial and abaxial surfaces of freshly picked Common Sage leaves (left), and the dehydrated product (right).

Figure 14. Photograph of freshly picked Common Sage leaves: adaxial revealing midrib and pinnate vascular bundles, and the abaxial revealing full vascular system (left). Finished solar dehydrated leaf product exhibiting LRS = 4 (right).

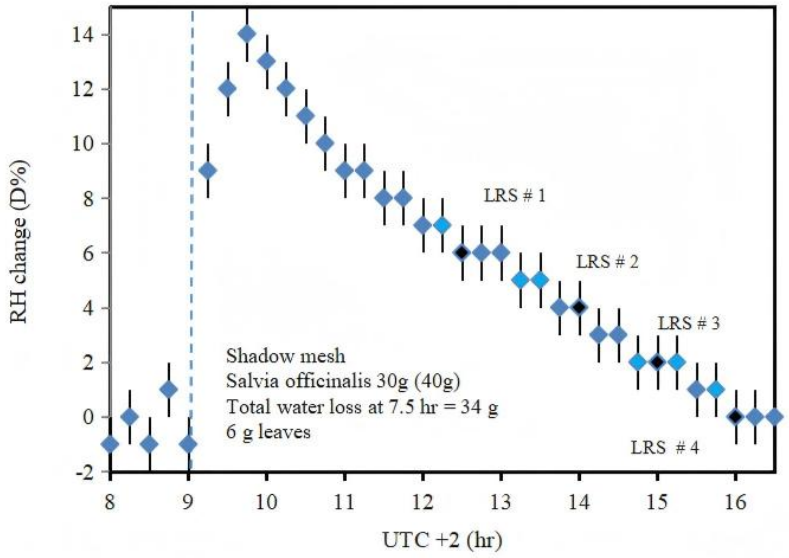

Figure 13. SBC-d and agricultural shadow-mesh solar dehydration A minus B RH data for Common Sage leaves in triple-stacked frames.

Note: Black-filled diamonds are LRS observations.

Adaxial Abaxial LRS = 4

Figure 14. Photographs of freshly picked Sweet Basil showing visible midrib and pinnate vascular bundles (left) and at 5 h of solar dehydration, t = 2 p.m (right).

5. SBC-d unloaded baseline model and leaf moisture component

In this section, the variation in the repeating SBC-d unloaded RH time series data across all four Lamiaceae leaf genera dehydration studies is explored to determine whether the data are sufficiently reliable as a target baseline for endpoint detection purposes. This is performed in Microsoft Excel using the A minus B array calculation. For this goal, the target baseline (column D) needs to be robust, not only as a baseline measurement used one day prior to the dehydration process, but also to cover an extended leaf dehydration period of a few months. In this work, the SBC-d unloaded RH time series data in **Figures 3**, **6**, **9**, and **12** are averaged for the days: 7.5.2025, 5.7.2025, 15.7.2025 and 24.7.2025. Then, a best-fit trend-line is fitted to the data to produce a 0D-model along with its variance. The results of these computations are shown in **Figure 15**.

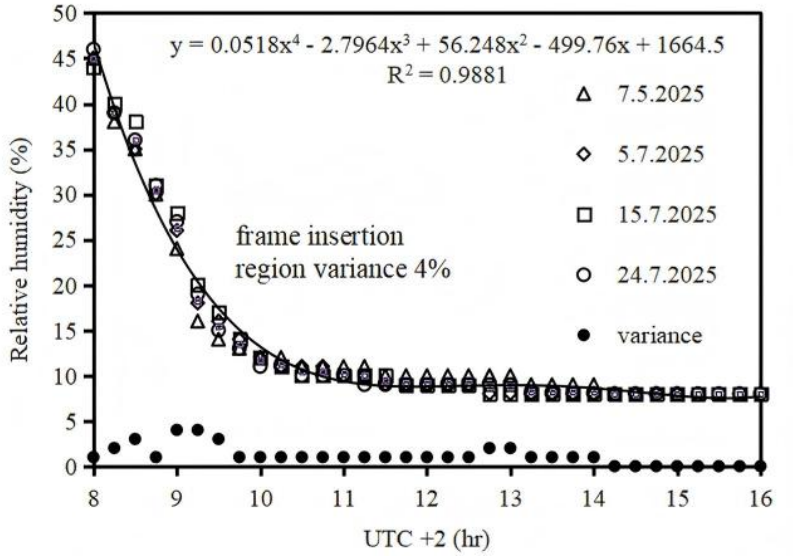

Figure 15. Unloaded SBC-d times series data (open: triangles, diamonds, circles, and squares), variance (black-filled circles), and 4th-order polynomial model of averaged RH data (Poly. (Average)).

Now consider the regression analysis of the four averaged datasets, which yields a best-fit $R^2 = 0.9881$ for a 4th-order polynomial function (black line labeled—poly. (Average)). The second best-fit is $R^2 = 0.7528$ for a power function, and the least best-fit is $R^2 = 0.6116$ for a natural logarithm function. The logarithm and power coefficients of these functions are given in **Appendix A**. Now consider the regression analysis of the four averaged datasets, which yields a best-fit $R^2 = 0.9881$.

The variance between the 4th-order polynomial 0D-model and the original data points (black-filled circles) shows that the main variance is associated with the preheating period, t = 8 to 9 a.m., and with the triple-stacked frames are inserted, t = 9 to 10 a.m. This is followed by a local RH variance of 1% at t = 12.75 to 1 p.m. It is reasonable to assume that the first variance is most likely caused by the varying moisture within the SBC-d, which the preheating period is designed to remove. The second variance is strongly associated with the windows opening and closing. The third variance, however, is more difficult to identify. Possible candidates for this may include, but are not limited to, quantization error due to low the resolution of the RH meter, or a delayed moisture diffusion coming from the SBC-d walls. Towards the extreme end of the polynomial curve (t = 4 to 4.5 p.m.), where the top frame leaves are judged to be dehydrated, the variance from the 0D-model is zero and may be considered a 0D-endpoint model baseline. In the real 3-dimensional world, the 27 L volume SBC-d incorporates a triple-stacked frame, where the leaves in the middle and bottom frames are partially hidden from the Sun's illumination. From experimental observation these leaves require further drying of approximately 1 h. **Table 3** lists the leaf-drying times and water-loss rates for the 0D-model (top frame) and for all the leaves in triple-stacked frames, and shows that for the four leaf types study described here is that the water loss rate is some 4.0 to 4.6 g per hour for both top frame and triple-stacked frames. However, a difference is observed when comparing Basil and Common Sage leaves, where an additional 1 h was required for drying the latter, resulting in a lower water

loss rate of 3.8 to 4 g per hour. The non-observable diffidence in the Bay leaf data may be accounted for by the insufficient measurement of the Bay leaf water content (28 %) as compared to the Basil (86 %) and Sage (76 %). Nevertheless, the outcome does show that for real-time HR using one measurement location within the SBC-d the 0D-model requires informed supervision to match the entire quantity of leaves being dehydrated.

Table 3. Unsupervised 0D-endpoint model and supervised endpoint model.

Leaf (water content)	0D-endpoint mode time (h)	0D-model water loss rate (g per h)	Triple-stacked endpoint time (h)	Triple-stacked water loss rate (g per h)
Female Bay (28%)	3	4	3	4
Sweet Basil (86%)	6	4.5	7	3.8
Greek Basil (86%)	6.5	4.6	7.5	4
Common Sage (76%)	7.5	4.5	8.5	4

6. State-space projection of Lamiaceae leaf rolling score and leaf shrinkage score

The accumulated information from the four Lamiaceae leaf solar dehydration studies allows LRS and leaf shrinkage to be plotted in state-space (**Figure 16**) for the first time. When comparing the leaf genera data, it is essential to note that the solar dehydration parameters for Basil and Common Sage were adjusted to the initial Bay leaf study, which has the largest average leaf area (47 cm^2) and the lowest leaf water content (28%). With this criterion, the Bay leaf data (black-filled circles with dashed line) forms a reference vector, with no observable leaf shrinkage. Where the LRS varies from 0 to 1, the leaves are suitable for direct culinary purposes. Beyond this range LRS values increase to 2 and 3, with the leaves becoming crisp, making them unsuitable for direct culinary use. This simple vector allows a meaningful comparison with the high water content leaves of Common Sage (76%) and the two Basil leaf (86%).

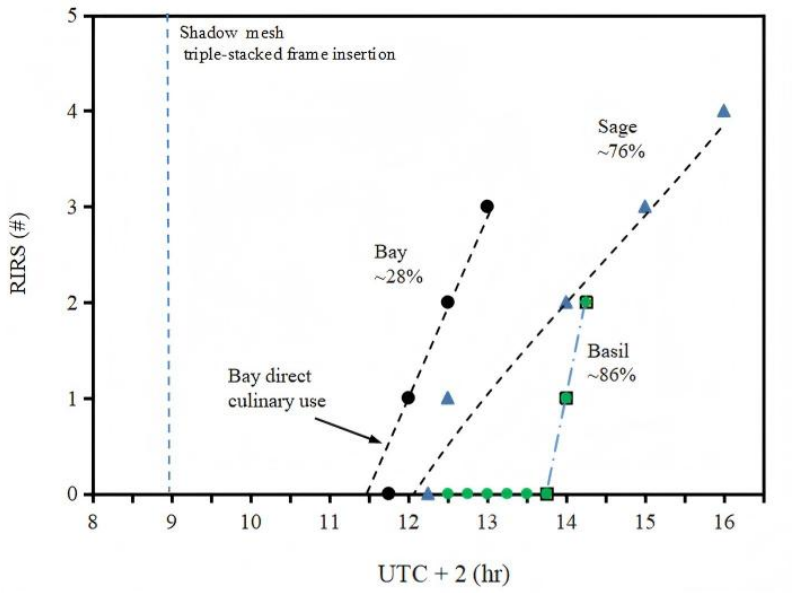

Figure 16. State-space projection of LRS and leaf shrinkage (green-filled circles). The tend-lines are intended to guide the eyes only.

Consider first the Common Sage that has a leaf area of approximately 31 cm^2, annotated here as blue-filled triangles with a natural logarithm function trend-line. These leaves exhibit an onset of leaf rolling some 15 min beyond the Bay Leaves without an indefinable shrinkage period. In addition, the Sage leaves exhibit a greater degree of leaf rolling (LRS = 4).

The Sweet and Greek Basil, which have an average leaf area of 20 cm^2 and 5 cm^2 respectively, exhibit leaf shrinkage, which typically begins at a point where the Bay and Common Sage start to reveal leaf rolling. This shrinkage response extends by approximately 90 min before the onset of leaf rolling

Given this emerging leaf rolling and shrinkage state-space picture of the four leaf types, it is reasonable to hypothesis there is a general area-preserving behavior between leaves and branching vascular systems as described by West, Brown, and Enquist [40, 41]. That is, the sum of the cross-sectional areas of the daughter branches equals that of the parent branch, from which it may be hypothesized that the hydraulic dynamics that is produced by the osmotic and vapor pressure is defined by the initial and finial diameters of the branching of the vascular system. Hence the larger the leaf area the greater the midrib cross-section area, as a result there is proportionally larger and stronger tertiary reticulated vascular bundles, when compared to the smaller leaf area of Basil leaves. More recently Agutter and Tuszynski [42] has advanced this virtual fractal network theory by suggesting structural resistance must also influences fluid flow rate in the finest branches of the network.

Following this reasoning, as the number of branches increases in geometric proportion, their size geometrically decreases (midrib → pinnate → venules) along with a corresponding decrease in rigidity and strength. Thus, venules will be the first to collapse when mesophyll and bulliform cells lose their turgor pressure under a given critical DSD environmental condition. Bay and Sage leaves with their large midrib and pinnate veins cross-sectional areas protect the leaf-blade from mechanical bending forces to a given point beyond which the continuous water moisture removal [when the sun is shining] induces mesophyll and bulliform cells structural adjustment that generate further mechanical force that is sufficient to bend the pinnate veins and the onset of leaf rolling in the leaf-blade. In contrast, Basil leaves with their high water content (86%) provide hydrostatic support around the skeletal vascular system, which fails under a rapid dehydrating environment as found in the DSD, resulting in leaf-blade collapse and shrinkage. As the failing process precedes the leaf epidermis bends the pinnate veins and venules, along with their protecting living collenchyma cells, to produce the characteristic leaf rolling appearance. A more detailed investigation of these observations, however, requires information on the biomechanical properties of the vascular bundles (Read and Stokes [43]). Nevertheless, state-space representation of leaf morphological change may provide an insight into the underlying dehydration process.

7. Comparison with other leaf solar dehydration studies

The accumulated SBC-d Lamiaceae leaf dehydration times allows to some degree a meaningful comparison with other Lamiaceae leaf dehydration times in other DSD

and ISD systems and geographical locations. However, it is important to note that such comparison is most likely to be convoluted by the differences in solar irradiance conditions, dryer geometry and airflow mechanisms. Given this qualification, the bar chart in **Figure 17** reveals reported dehydration times for: Bay [4], Sweet Basil [5], and Common Sage [2, 3], along with the four Lamiaceae leaves dehydrated in the SBC-d (color code green and red).

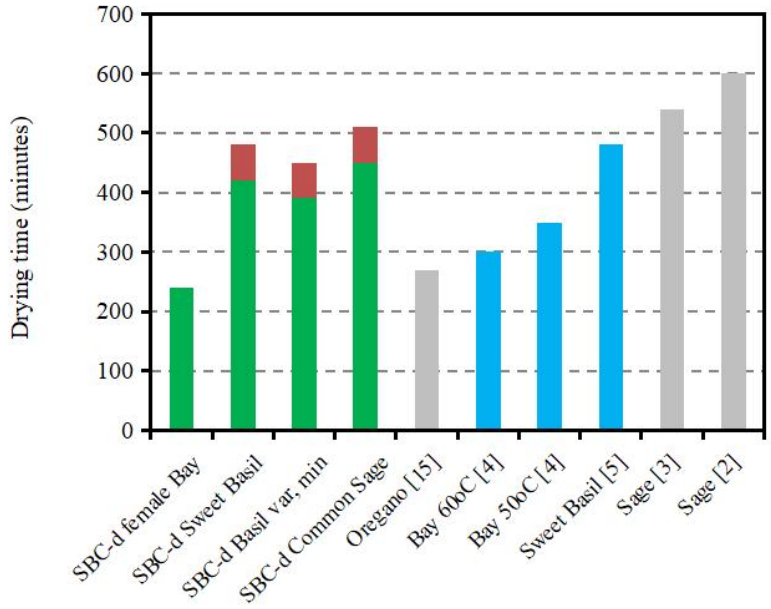

Figure 17. A comparison of reported Lamiaceae leaf dehydration times within DSD (grey) and ISD (blue).

Note: The green-filled bars correspond to the unsupervised 0D-model, and the red-filled portion of the bars correspond to the supervised model.

The comparative drying times for the unsupervised 0D-model and the supervised model are summarized as follows. For the unsupervised 0D-model, female Bay leaf dehydration times within the SBC-d has an apparent lower drying time (240 min) than Bay leaf drying times at either 60 ℃ (300 min) at 50 ℃ (350 min) within an ISD system under the Algerian Sun (36° N, 3° W) [4]. The Oregano leaves in a DSD coupled with agricultural shadow-mesh (Mexico: 17.6° N, 92° W) have a comparable drying time of 270 min [19], similar to this repoted drying time in this work. Sweet and Greek Basil leaves also have shorter drying times (390 to 430 min) within the SBC-d when compared to Sweet Basil dehydrated times (480 min) within an ISD system (Egypt: 30°47′ N, 30° W). The comparison between DSD and ISD is further exemplified when comparing dying times of Common Sage in the SBC-d (450 min) to Common Sage within an ISD system (600 min, located in Egypt: 30.5° N, 32.27° E) [2], and 550 min in Egypt: 30° N, 31.2° E) [3]. For the supervised leaf model, the drying times of Basil leaves are within 10 min of those reported by Shalaby et al. [5]. Furthermore, Common Sage total drying times have also increased to 510 min, some 30 to 70 min shorter than [2, 3].

From this limited comparative the drying time data it can be observed that there is an observable difference in leaf dry time across the types of solar device used, it geographic location and the leaf type being dried; all of which point the need for further

investigation.

8. Conclusion

This work presents a new and novel form of off-grid DSD dehydration of Lamiaceae culinary leaves (Bay, Sweet and Greek Basil, and Common Sage) using load (leaf) and unloaded (empty) DSD, (termed here as SBC-d) RH measurements as the metric for leaf dryness. The solar dehydration study is constructed with four main aims (objectives).

The first aim acknowledges that RH measurements are likely to be sensitive to ambient variability, leakage/ventilation, and temperature effects. Therefore, all dehydration experiments normalized to one DSD that is converted from a family sized (27 L) SBC on the island of Crete (35.31° N, 24.31° E, altitude 150 m) in the Eastern Mediterranean Sea during the months May through July 2025. The SBC-d is operated in the open green-house principle, where passive air flow ventilation is used to accumulated heat and moisture from SBC-d. In this mode of operation the leaves are placed on vertically tripe-staked dehydration frames.

The second aim was to visually identify leaf solar dehydration morphological induced changes which are not conducive to achieving the final dehydrated leaf product. For the experimental period (May through July) it was found that green agricultural shadow-mesh covers the SBC-d was needed to limit the intense the Sun's irradiance and prevent leaf rolling and shrinkage of four different culinary Lamiaceae leaf types.

The third aim was to develop a leaf dehydration endpoint methodology based on a single location point RH and temperature measurements, with the time dependent data complied within a Microsoft Excel software environment. Using this approach it was found that an A minus B mathematical operation of the unloaded and loaded RH measurements reveals water vapor released from the leaves during a one day period dehydration process can be monitored and used as an 0D-model endpoint signal for leaves placed on the top frame prior to the onset of leaf rolling and shrinkage. However, leaves placed on the mid and bottom frames are partially shaded from direct solar illumination dry at a slower rate, therefore convoluting the 0D-model endpoint signal. Thus 0D-model endpoint requires supervision to obtain a real-world endpoint.

Acknowledging the SBC-d is a form of sustainable green technology with drawbacks with regard to leaf direct solar illumination, the fourth aim of this work is to develop a state-space-model that could be used to aid the supervision the 0D-model and a real-world leaf endpoint for all the leaves within the SBC-d. Monitoring beyond the 0D-model leaf dehydration endpoint time-stamp it was found that an additional 1 h solar processing for the leaves placed on the middle and bottom frames. This outcome demonstrates that the 0D-model requires supervision for all the leaves to be judged to be sufficiently dehydrated. When differentiating between the drying times of the Lamiaceae culinary leaves types, it is found that the leaf dehydration time for leaves on the top frame follows the inherent water content of the leaf; that is female Bay requiring the least drying time and Basil leaves the greatest dehydration time. In all cases dehydration time was within one solar drying day.

In addition, the projection of leaf rolling score and leaf shrinkage in state-space

reveals a meaningful comparison between different Lamiaceae leaf responses to a SBC-d dehydration process, which to the knowledge of the authors has not previously been reported. With this emerging picture, solar dehydration mechanisms can be tested. All the regression analysis of the SBC-d dehydration studies are tabulated in **Appendix A** that allow researchers to consult and build upon on the data to producing realistic SBC-d leaf dehydration models, thereby leading to the improvement of scientific knowledge of leaf solar dehydration stress.

The research findings of this work suggest a number of potential directions and scope for future off-grid SBC-d research: firstly, extend the study of solar leaf dehydration to Rosemary and Thyme where there is a need to keep their relative small leaves on their parent branches to prevent them falling through support structure of the dehydration frames. This would mean scaling-out, the SBC-d design to incorporate the necessary branch length (30–40 cm) to maintain batch leaf throughput. Thirdly, utilize building information modelling (BIM) software to identify and capture the shadowing on leaves placed on frames below the top dehydration frame. Fourth, correlate the observed visual solar dehydration stress to specific leaf colour, microscopic analysis of leaf vascular tissues, mechanical bending tests, and cellular dehydration imaging so that a better understanding of the SBC-d environment may be established.

Author contributions: VJL, JFL and DPD conceived and planned the solar experiments. JM contributed to the environmental approach taken though out the solar experiments. VJL wrote the manuscript with input from all authors. All authors have read and agreed to the published version of the manuscript.

Funding: This work received no external funding.

Institutional review board statement: Not applicable.

Informed consent statement: Not applicable.

Data availability statement: The data used in this study are available from the corresponding author upon reasonable request.

Conflict of interest: The authors declare they have no conflict of interest.

AI use statement: The authors declare that no artificial intelligence (AI) tools were used in the preparation of this manuscript.

References

1. Kerr BP. The Expanding World of Solar Box Cookers. Kerr BP (self-published); 1991.
2. Hassanain AA. Drying sage (*Salvia officinalis* L.) in passive solar dryers. Research in Agricultural Engineering. 2011; 57(1): 19–29. doi: 10.17221/14/2010-RAE
3. Imam AI, Elhamed RSA, Mohammed MHM, et al. Evaluation of different drying methods of sage leaves, bioactive compounds content and its utilization as a natural additive to flatbread. Future Journal Agriculture. 2013; 1: 50–75.
4. Ouafi N, Benaouda N, Moghrani H, et al. Experimental analysis of solar drying kinetic of Algerian bay leaves (*Laurus nobilis* L.). Journal of Renewable Energies. 2024; 19(2): 251–264. doi: 10.54966/jreen.v19i2.565
5. Shalaby SM, Darwesh M, Ghoname MS, et al. The effect of drying sweet basil in an indirect solar dryer integrated with phase change material on essential oil valuable components. Energy Reports. 2020; 6: 43–50. doi: 10.1016/j.egyr.2020.10.035

6. Jayasuriya H, Pathare PB, Al-Attabi Z, et al. Drying Kinetics and Quality Analysis of Coriander Leaves Dried in an Indirect, Stand-Alone Solar Dryer. Processes. 2023; 11(6): 1596. doi: 10.3390/pr11061596
7. Bennamoun L, Dakhmouche S, Bennacer, S, et al. Exploring solar drying of henna (*lawsonia inermis*) and its effect on the bioactivities. Drying Technology. 2024; 2(10): 1540–1551.
8. Ndukwu MC, Akpan G, Okeahialam AN, et al. A comparison of the drying kinetics, energy consumption and colour quality of drying medicinal leaves in direct-solar dryer with different colours of collector cover. Renewable Energy. 2023; 216: 119076. doi: 10.1016/j.renene.2023.119076
9. Tonadi E, Niharman, Wiranto B. Performance analysis of solar photovoltaic thermal (PV/T) dryer for drying moringa leaf. JTTM: Jurnal Terapan Teknik Mesin. 2024; 5(1): 90–96. doi: 10.37373/jttm.v5i1.777
10. Papu S, Sweta S, Singh BR, et al. The Drying Characteristics of Amaranth Leaves under Greenhouse Type Solar Dryer and Open Sun. Greener Journal of Agricultural Sciences. 2014; 4(6): 281–287. doi: 10.15580/GJAS.2014.6.040314174
11. Akbar FN, Mahmood S, Mueen-ud-din G, et al. Exploring the Effects of Drying Method and Temperature on the Quality of Dried Basil (Ocimum basilicum L.) Leaves: A Sustainable and Eco-Friendly Drying Solution. Resources. 2024; 13(9): 121. doi: 10.3390/resources13090121
12. Dhande A, Agarwal M, Agarwal GD. Energy and enviro-economic (3E) assessment of greenhouse solar dryer (GHSD) for drying and quality evaluation of medicinal Ocimum sanctum leaves: A sustainable path for preservation. Environmental Progress & Sustainable Energy. 2024; 43(6): e14484. doi: 10.1002/ep.14484
13. Danso-Boateng E. Effect of drying methods on nutrient quality of basil (*ocimum viride*) leaves cultivated in ghana. International Food Research Journal. 2023; 20(4): 1569–1573.
14. Abdulmujeeb A, Garba MM, Sokoto AM, et al. Thermal performance of dual-operated solar cooking and drying system. Fudma Journal of Sciences. 2023; 7(4): 298–306. doi: 10.33003/fjs-2023-0704-1930
15. Law VJ, Lalor JF, Dowling DP. Inclined Window Solar Box Cooker with One External Reflector Designed for the Mediterranean Latitudes. Journal of Power and Energy Engineering. 2024; 12(11): 1–33. doi: 10.4236/jpee.2024.1211001
16. Lalor JF, Law VJ, Dowling DP. Winterizing and Use of a Solar Box Cooker on the Island of Crete, Greece. American Journal of Analytical Chemistry. 2025; 16(03): 23–41. doi: 10.4236/ajac.2025.163003
17. Law VJ, Lalor JF, Magnes J., et al. Solar box recovery of mixed-wax candle fragments and reuse on the island of Crete. Energy Storage and Conversion. 2026. doi: 10.59400/esc4099
18. Kumar M, Sansaniwal SK, Khatak P. Progress in solar dryers for drying various commodities. Renewable and Sustainable Energy Reviews. 2016; 55: 346–360. doi: 10.1016/j.rser.2015.10.158
19. Castillo-Téllez M, Martínez OS, Miranda-Mandujano E, et al. Solar drying of oregano leaves (Plectranthus amboinicus , Lour): Analysis of experimental performance under a tropical climate. Energy Exploration & Exploitation. 2024; 42(5): 1895–1921. doi: 10.1177/01445987241234389
20. Law VJ, Dowling DP. Microwave-Assisted Transition Metal Nanostructure Synthesis: Power-Law Signature Verification. American Journal of Analytical Chemistry. 2023; 14(8): 326–349. doi: 10.4236/ajac.2023.148018
21. Law VJ, Dowling DP. Green Chemistry Allometry Test of Microwave-Assisted Synthesis of Transition Metal Nanostructures. American Journal of Analytical Chemistry. 2023; 14(11): 493–518. doi: 10.4236/ajac.2023.1411029
22. Giménez L, Chatterjee A, Torres G. A state-space approach to understand responses of organisms, populations and communities to multiple environmental drivers. Communications Biology. 2021; 4(1): 1142. doi: 10.1038/s42003-021-02585-1
23. Uikey J. Reviewing of plant belonging to lamiaceae family. International Journal of Scientific Development and Research. 2024; 9(3): 186–191.
24. Joshi P, Rawat S, Pandey P, et al. Study on phytochemical diversity of Lamiaceae: Promising leads in anti-malarial drug development. International Journal of Botany Studies. 2024; 9(12): 20–25.
25. Serebrynaya FK, Nasuhova NM, Konovalov DA. Morphological and Anatomical Study of the leaves of Laurus nobilis L. (Lauraceae), growing in the Introduction of the Northern Caucasus region (Russia). Pharmacognosy Journal. 2017; 9(4): 519–522. doi: 10.5530/pj.2017.4.83
26. Pysklynets I, Makhinya L. Anatomical and phytochemical study of Ocimum basilicum L. leaves of two popular varieties in Ukraine. The Ukrainian Scientific Medical Youth Journal. 2024; 149(3): 156–165. doi: 10.32345/USMYJ.3(149).2024.156-165
27. El-Sahhar KF, Nassar RM, Farag HM. Comparative botanical studies of some Salvia species (Lamiaceae) grown in egypt. II. anatomical and molecular characteristics. Research Journal of Pharmaceutical, Biological and Chemical

Sciences. 2017; 8(4): 600–619.
28. Özdemir C, Baran P, Aktas K. Anatomical studies in *Salvia viridis* L. (Lamiaceae). Bangladesh Journal of Plant Taxonomy. 1970; 16(1): 65–71. doi: 10.3329/bjpt.v16i1.2748
29. Yurdakul M, Leylak C, Buzrul S. Use of Excel in food science 2: Non-linear regression. Food and Health. 2020; 199–212. doi: 10.3153/FH20021
30. Buzrul S. On The Pros and Cons of Using Excel for Regression Analysis. Turkish Journal of Agriculture - Food Science and Technology. 2024; 12(s2): 2234–2241. doi: 10.24925/turjaf.v12is2.2234-2241.6931
31. Hernández E, Montero G, Lambertb A, et al. Influences of the Relative Humidity in the Monthly Invoicing in Constructions of Warm Climates Using the Hour-degree Methodology. Energy Procedia. 2014; 57: 2052–2061. doi: 10.1016/j.egypro.2014.10.170
32. Ali Z, Merrium S, Habib-ur-Rahman M, et al. Wetting mechanism and morphological adaptation; leaf rolling enhancing atmospheric water acquisition in wheat crop—A review. Environmental Science and Pollution Research. 2022; 29(21): 30967–30985. doi: 10.1007/s11356-022-18846-3
33. Yavas I, Jamal MA, Ul Din K, et al. Drought-Induced Changes in Leaf Morphologyand Anatomy: Overview, Implicationsand Perspectives. Polish Journal of Environmental Studies. 2023. doi: 10.15244/pjoes/174476
34. Fen LL, Ismail MR, Zulkarami B, et al. Physiological and molecular characterization of drought responses and screening of drought tolerant rice varieties. Bioscience Journal. 2015; 31(3): 709–718. doi: 10.14393/BJ-v31n3a2015-23461
35. Latif A, Ying S, Cuixia P, et al. Rice Curled Its Leaves Either Adaxially or Abaxially to Combat Drought Stress. Rice Science. 2023; 30(5): 405–416. doi: 10.1016/j.rsci.2023.04.002
36. Guo K, Liu M, Vella D, et al. Dehydration-induced corrugated folding in Rhapis excelsa plant leaves. Proceedings of the National Academy of Sciences. 2024; 121(17): e2320259121. doi: 10.1073/pnas.2320259121
37. Klingenberg CP. Size, shape, and form: Concepts of allometry in geometric morphometrics. Development Genes and Evolution. 2016; 226(3): 113–137. doi: 10.1007/s00427-016-0539-2
38. Stumpf MPH, Porter MA. Critical Truths About Power Laws. Science. 2012; 335(6069): 665–666. doi: 10.1126/science.1216142
39. Andriani P, McKelvey B. From Gaussian to Paretian Thinking: Causes and Implications of Power Laws in Organizations. Organization Science. 2009; 20(6): 1053–1071. doi: 10.1287/orsc.1090.0481
40. West GB, Brown JH, Enquist BJ. A General Model for the Origin of Allometric Scaling Laws in Biology. Science. 1997; 276(5309): 122–126. doi: 10.1126/science.276.5309.122
41. West GB, Brown JH, Enquist BJ. A general model for the structure and allometry of plant vascular systems. Nature. 1999; 400(6745): 664–667. doi: 10.1038/23251
42. Agutter PS, Tuszynski JA. Analytic theories of allometric scaling. The Journal of Experimental Biology. 2011; 214: 1055–1062.
43. Read J, Stokes A. Plant biomechanics in an ecological context. American Journal of Botany. 2006; 93(10): 1546–1565. doi: 10.3732/ajb.93.10.1546

Appendix A

Table A1. Microsoft Excel trend-line fit to time series data.

Function and fit	SBC-d unloaded Air temperature (°C)	SBC-d unloaded RH (%)	SBC-d loaded RH (%)
Bay			
Logarithm	$y = 11.007\ln(x) + 22.101$	$y = -11.62\ln(x) + 42.524$	$y = -11.39\ln(x) + 44.594$
R^2	0.9922	$R^2 = 0.8903$	0.9859
Power	$y = 24.867x^{0.2706}$	$y = 50.977x^{-0.573}$	$y = 56.681x^{-0.537}$
R^2	0.9808	$R^2 = 0.9291$	0.9695
n^{th}-order polynomial	$y = -0.0645x^2 + 2.8366x + 25.009$	$y = 0.0003x^4 - 0.0265x^3 + 0.7864x^2 - 9.9561x + 55.792$	$y = 0.0005x^4 - 0.0299x^3 + 0.7047x^2 - 8.0044x + 51.924$
R^2	0.9683	0.9835	0.9949

Table A1. *Cont.*

Function and fit	SBC-d unloaded Air temperature (°C)	SBC-d unloaded RH (%)	SBC-d loaded RH (%)
Sweet Basil			
Logarithm	$y = 8.7846\ln(x) + 28.818$	$y = -10.64\ln(x) + 41.204$	$y = -10.91\ln(x) + 47.339$
R^2	0.9686	0.8516	0.975
Power	$y = 31.112x^{0.19}$	$y = 50.236x^{-0.572}$	$y = 67.759x^{-0.536}$
R^2	0.9694	0.9076	0.89
n^{th}-order polynomial	$y = -0.037x^2 + 2.0006x + 31.687$	$y = 0.0002x^4 - 0.019x^3 + 0.6358x^2 - 9.1236x + 55.987$	$y = 8E\text{-}05x^4 - 0.0069x^3 + 0.2237x^2 - 3.8959x + 45.82$
R^2	0.9892	0.9872	0.9757
Greek Basil			
Logarithm	$y = 9.29\ln(x) + 27.45$	$y = -10.82\ln(x) + 41.363$	$y = -11.51\ln(x) + 47.67$
R^2	0.9756	0.8812	0.974
Power	$y = 29.952x^{0.2041}$	$y = 51.943x^{-0.588}$	$y = 70.033x^{-0.581}$
R^2	0.9789	0.9345	0.9005
n^{th}-order polynomial	$y = -0.0407x^2 + 2.1378x + 30.493$	$y = 0.0002x^4 - 0.019x^3 + 0.6192x^2 - 8.7726x + 54.499$	$y = 9E\text{-}05x^4 - 0.0068x^3 + 0.2192x^2 - 4.0099x + 46.24$
R^2	0.9893	0.9908	0.9782
Common Sage			
Logarithm	$y = 35.261\ln(x) - 35.938$	$y = -36.76\ln(x) + 104.7$	$y = -42.67\ln(x) + 124.42$
R^2	0.8814	0.6221	0.931
Power	$y = 7.8989x^{0.7503}$	$y = 2{,}164.1x^{-2.117}$	$y = 4{,}489.8x^{-2.26}$
R^2	0.8345	0.7471	0.9927
n^{th}-order polynomial	$y = -0.59x^2 + 17.308x - 68.1$	$y = 0.0409x^4 - 2.2582x^3 + 46.456x^2 - 422.6x + 1443.1$	$y = 0.0148x^4 - 0.8092x^3 + 16.669x^2 - 155.49x + 573.26$
R^2	0.9911	0.9841	0.9888